24th EUROPEAN ROTORCRAFT FORUM
Marseilles, France - 15th-17th September 1998

REFERENCE: DY08

ROTARY-WING AEROELASTIC SCALING AND ITS APPLICATION TO ADAPTIVE MATERIALS BASED ACTUATION

P.P. Friedmann*
Mechanical and Aerospace Engineering Department
University of California
Los Angeles, California 90095-1597

The aeroelastic scaling problem is revisited and it is shown that classical aeroelastic scaling relations, developed for flutter, need to be extended when dealing with modern aeroelastic applications, involving controls and adaptive materials based actuation. For such problems a novel two pronged approach is presented that produces refined aeroelastic scaling laws by a judicious combination of the classical approach with more sophisticated computer simulations. It is also shown that the rotary-wing equivalent to fixed-wing aeroelastic scaling, based on typical cross-section concepts, is the offset hinged spring restrained blade model. Scaling laws for the rotary-wing aeroelastic and aeroservoelastic problem are obtained. These scaling requirements imply that scale model tests, conducted on small models intended to demonstrate active control of vibration using adaptive materials based actuation, use very flexible models that often disregard aeroelastic scaling. Thus, the extension of these results to the full scale configuration is difficult.

LIST OF SYMBOLS

a Lift curve slope
a_h Nondimensional elastic axis location measured from midchord
b Blade semichord
$C(k)$ Theodorsen's lift deficiency function
C_{d0} Drag coefficient of blade
C_l Lift coefficient
C_m Pitching moment coefficient about elastic axis
C_h Hinge moment coefficient
c_β Nondimensional flap hinge location
e Blade offset
g_{SF}, g_{SL}, g_{ST} Damping coefficients
h plunge displacement
H, $\bar{H}$ Hinge moment, and nondimensional hinge moment per unit span
H_β Hinge moment
I_b Blade flapping inertia
I_f Blade feathering inertia
I_{MB_2}, I_{MB_3} Principal moments of inertia per unit length of blade about cross-sectional axes
I_α Airfoil moment of inertia about elastic axis, with undeflected flap
I_β Flap moment of inertia about hinge axis
k Reduced frequency ($\omega b/V$)
K_h, K_α, K_β Spring constants, restraining bending, torsion and control flap rotation
K_β, K_ζ, K_ϕ Root spring stiffness in flap, lag and torsion respectively, proportional to blade bending and torsional stiffnesses
L Lift per unit span
m Mass per unit length of blade, or wing
M Mach number
M_m, M_w Mass for model and full scale configuration, respectively
M_α Pitch moment per unit span
M_β, M_ζ, M_ϕ Elastic restoring moments in flap, lag and torsion, respectively
$[M]$, $[K]$ Mass and stiffness matrices for three degree of freedom airfoil system
n_L, n_M, n_T Scaling factors for length, mass and time
P, $\bar{P}$ Power and nondimensional power per unit length, respectively
Q_I, Q_A, Q_D Inertia, aerodynamic and damping moments on blade
$\{q\}$ Generalized degrees of freedom vector
R Rotor radius
r_α, r_β Radius of gyration of airfoil and control

*Professor

	flap, respectively
S_α, S_β	Static moment of airfoil and flap, respectively
t	Time
$\bar{t}$	Nondimensional time, $(\omega_\alpha t)/2\pi$
$\bar{t}_1$, $\bar{t}_2$	Nondimensional time in power calculations
$T_1 - T_{19}$	Constants used in Theodorsen type aerodynamics
T_m, T_w	Time for model and full scale configuration respectively
$\bar{U}$	Nondimensional speed $(V/b\omega_\alpha)$
V	Velocity of flight
x_A	Offset between elastic center and aerodynamic center in blade cross section
x_I	Offset between elastic center and the mass center in blade cross section
x_α	Nondimensional static moment of airfoil about elastic axis, (S_α/mb)
x_β	Nondimensional flap static moment about hinge, (S_β/mb)
β, β_0	Control flap deflection angle and amplitude, respectively, also blade flapwise bending degree of freedom
β_p	Precone angle
ζ, ϕ	Blade lag and torsional displacements
Θ_G	Blade geometric pitch angle
λ	Inflow ratio
ρ_A	Density of air
μ	Advance ratio
$\bar{\mu}$	Mass ratio, $m/(\pi\rho b^2)$
ξ, ξ_0	Nondimensional plunge displacement, h/b and amplitude, respectively
ϕ_1, ϕ_2	Phase angles for torsional and trailing edge flap degrees of freedom, respectively
ψ	Azimuth angle
ω_h, ω_α, ω_β	Uncoupled natural frequencies associated with the three degree of freedom typical cross section, respectively
ω	Flutter frequency
Ω	Rotor RPM
$(\dot{})$	Derivatives with respect to time

1 INTRODUCTION

Approximately fifteen years ago, active materials have been identified as potentially useful for a variety of aerospace applications as both sensors and actuators, and since then the area of "smart structures" or "adaptive structures", combining active materials, controls and microprocessors has been burgeoning. Many important applications are related to aeroelasticity, for both fixed wing and rotary-wing aircraft, and a number of survey articles on these topics have been written [10, 14, 22, 25, 31, 53].

Active materials have been applied to a variety of aeroelastic problems, such as: static aeroelasticity, wing-lift effectiveness, and divergence [47, 54] supersonic panel flutter [44,45] flutter and dynamic load alleviation [24, 28, 30] vibration reduction in helicopter rotors [8, 48, 49] wing/store flutter suppression [21]. The principal emphasis in this paper will be on the rotary-wing applications of adaptive materials.

It is useful to mention that fixed wing applications of adaptive materials have been aimed primarily at the flutter suppression problem and to a lesser extent to the vibration or load alleviation problem. A limited number of studies also have addressed the gust load alleviation problem in wings, as well as the tail buffet alleviation problem in fighter type aircraft. In contrast the primary applications envisioned for adaptive materials in the rotary-wing vehicles are: the vibration alleviation problem in rotors, blade tracking problem, blade vortex interaction (BVI) alleviation problem, and possibly the reduction of noise associated with BVI.

Demonstration of feasibility of actuators built from adaptive materials for aeroelastic applications, for both fixed-wing and rotary-wing vehicles, is usually carried out by constructing small, scaled models, employed in wind tunnel tests. Once feasibility of a particular approach or concept is demonstrated, construction of larger, or even full scale models is often recommended. However, little attention is paid to aeroelastic scaling laws that allow one to relate behavior of the scale model to that of the full-scale configuration.

During the last thirty years aeroelastic scaled wind tunnel models have been widely used in testing, and aeroelastic scaling laws that enable one to relate wind tunnel test results to the behavior of the full scale system have played an important role in aeroelasticity. Such scaling laws have relied on dimensional analysis to establish a set of scaling parameters used for aeroelastically scaled models, suitable for wind tunnel testing [6, 26]. More refined laws can be obtained using similarity solutions, which represent closed form solutions to the equations of motion. However, these are impractical for complex aeroelastic problems [1, 2]. Furthermore, aeroelastic scaling laws have been aimed primarily at fixed-wing aeroelastic stability (i.e. flutter) testing [6] or rotary-wing aeromechanical stability (i.e. flutter and coupled rotor/fuselage instabilities) testing [26]. However, the applications envisioned for adaptive materials based actuation are aeroservoelastic applications involving actuators, sensors, and a controller. Also, such applications frequently depend on important quantities such as forces, moments, and actuator stroke required for flutter suppression or vibration alleviation. These situations are not covered by classical aeroe-

lastic considerations. Finally, it should be also noted that the rotary-wing aeroelastic problem is inherently nonlinear [18], thus the linear approach, used in the past [6,26], needs to be re-examined. Thus, it is evident that the aeroelastic scaling of these modern, complex aeroelastic configurations requires the development of more refined aeroelastic scaling laws.

The objectives of this paper are: (1) revisit aeroelastic scaling in the context of modern aeroelasticity. emphasizing active controls, and adaptive materials based actuation; (2) develop aeroelastic and aeroservoelastic scaling laws for rotary wing applications; and (3) examine several applications of adaptive materials based actuation to vibration reduction in rotorcraft, within the framework of aeroelastic scaling considerations.

2 AEROELASTIC SCALING REVISITED

The most detailed treatment of aeroelastic scaling laws is presented in Ch. 11 of Ref. 6, where the flutter problem of a typical cross section in incompressible flow is treated. Since then this important problem has received only limited attention in the literature [42,46], and most of the work, with the exception of Ref. [26], has focused on fixed-wing aeroelastic scaling. Recently, the problem of aeroelastic scaling has been revisited [14,15,41]. In Ref. 15 the aeroservoelastic problem of a typical airfoil in transonic flow and its scaling has been considered with considerable detail. The problem of aeroelastic and aeroservoelastic scaling in subsonic compressible flow, including adaptive materials based actuation was discussed in Ref. 41.

For completeness it is useful to examine first the aeroelastic scaling problem of a wing typical section, combined with a trailing edge control surface, depicted in Fig. 1. For this case the equation of motion can be written as [15]

$$mb^2[M]\{\ddot{q}\}+mb^2\omega_\alpha^2[K]\{q\} = \left\{ \begin{array}{c} -Lb \\ M_\alpha \\ H_\beta \end{array} \right\} = \rho b^4 \bar{U}^2 \omega_\alpha^2 \left\{ \begin{array}{c} -C_l \\ 2C_m \\ 2C_h \end{array} \right\} \quad (1)$$

It is useful to obtain first the scaling relations for incompressible flow, under the assumption of simple harmonic motion, and then extend these relations to a more general case. For the incompressible case, the aerodynamic loads can be written as

$$\begin{aligned} \left\{ \begin{array}{c} -L_b \\ M_\alpha \\ H_\beta \end{array} \right\} &= \rho b^4 \left[\begin{array}{ccc} -\pi & \pi a & T_1 \\ \pi a_h & -\pi(\frac{1}{8}+a_h^2) & -2T_{13} \\ T_1 & -2T_{13} & \frac{1}{\pi}T_3 \end{array} \right] \{\ddot{q}\} \\ &+ \rho b^3 V \left[\begin{array}{ccc} 0 & -\pi & -T_4 \\ 0 & \pi(a_h-\frac{1}{2}) & -T_{16} \\ 0 & -T_{17} & -\frac{1}{\pi}T_{19} \end{array} \right] \{\dot{q}\} \\ &+ \rho b^2 V^2 \left[\begin{array}{ccc} 0 & 0 & 0 \\ 0 & 0 & -T_{15} \\ 0 & 0 & -T_{19}\pi \end{array} \right] \{q\} \\ &+ \rho b^2 V^2 C(k) \left(\left[\begin{array}{ccc} 0 & -2\pi & -2T_{10} \\ 0 & 2\pi(\frac{1}{2}+a_h) & 2(\frac{1}{2}+a_h)T_{10} \\ 0 & -T_{12} & -T_{10}T_{12}/\pi \end{array} \right] \{q\} \right. \\ &\left. + \frac{b}{V} \left[\begin{array}{ccc} -2\pi & -2\pi(\frac{1}{2}-a_h) & -T_{11} \\ 2\pi(\frac{1}{2}+a_h) & 2\pi(\frac{1}{4}-a_h^2) & T_{11}(\frac{1}{2}+a_h) \\ -T_{12} & -T_{12}(\frac{1}{2}-a_h) & -T_{11}T_{12}/2\pi \end{array} \right] \{\dot{q}\} \right) \end{aligned} \quad (2)$$

where the nondimensional coefficients T_i are defined in Ref. 51, and they depend only on the nondimensional hinge location c_β and center of gravity a_h. Note that only $T_1 - T_{14}$ are independent and the additional T_i represent convenient combinations of the preceding T_i's.

The assumption of simple harmonic motion implies

$$\left\{ \begin{array}{c} \xi(t) \\ \alpha(t) \\ \beta(t) \end{array} \right\} = \left\{ \begin{array}{c} \xi_0 e^{i\omega t} \\ \alpha_0 e^{i\omega t+\phi_1} \\ \beta_0 e^{i\omega t+\phi_2} \end{array} \right\} \quad (3)$$

where ϕ_1 and ϕ_2 represent phase lag angles.

Combining Eqs. (1-3) and dividing by $mb^2\omega_\alpha^2$,

$$\begin{aligned} &-\xi_0 - x_\alpha \alpha_0 e^{i\phi_1} - x_\beta \beta_0 e^{i\phi_2} + \left(\frac{\omega_\alpha}{\omega}\right)^2 \left(\frac{\omega_h}{\omega_\alpha}\right)^2 \xi_0 = \\ &\qquad F_1(c_\beta, a_h, k, \bar{\mu}, \xi_0, \alpha_0, \phi_1, \beta_0, \phi_2) \\ &-x_\alpha \xi_0 - r_\alpha^2 \alpha_0 e^{i\phi_1} - \left[r_\beta^2 + (c_\beta - a_h)x_\beta\right] \beta_0 e^{i\phi_2} + \\ &\quad r_\alpha^2 \left(\frac{\omega_\alpha}{\omega}\right)^2 \alpha_0 e^{i\phi_1} = \\ &\qquad F_2(c_\beta, a_h, k, \bar{\mu}, \xi_0, \alpha_0, \phi_1, \beta_0, \phi_2) \\ &-x_\beta \xi_0 - \left[r_\beta^2 + (c_\beta - a_h)x_\beta\right] \alpha_0 e^{i\phi_1} - r_\beta^2 \beta_0 e^{i\phi_2} + \\ &\quad r_\beta^2 \left(\frac{\omega_\alpha}{\omega}\right)^2 \left(\frac{\omega_\beta}{\omega_\alpha}\right)^2 \beta_0 e^{i\phi_2} = \\ &\qquad F_3(c_\beta, a_h, k, \bar{\mu}, \xi_0, \alpha_0, \phi_1, \beta_0, \phi_2) \end{aligned} \quad (4)$$

Equations (4) allow one to establish aeroelastic scaling relations for the incompressible case. The primary quantities are mass M, length L, and time T. A convenient set of dimensionless quantities governing the problem can be extracted from Eqs. (4) and is given by $\xi_0 = h_0/b$, $\omega b/V = k$, $\bar{\mu} = m/\pi\rho b^2$, $\omega_h/\omega_\alpha =$

$\sqrt{[(K_h/m)/(K_\alpha/I_\alpha)]}$, $\omega_\beta/\omega_\alpha$, $\frac{\omega_\alpha}{\omega}$, r_α^2, r_β^2, c_β, a_h, $x_\alpha = S_\alpha/mb$, $x_\beta = S_\beta/mb$, α_0, β_0, ϕ_1 and ϕ_2. There are a total of sixteen nondimensional parameters. The first twelve can be expressed as various combinations of the physical quantities that depend on the primary variables M, L, and T, where the last four are pure nondimensional quantities. When dealing with the aeroelastic stability problem, which is homogeneous, the number of dimensionless ratios can be reduced by one by dividing through by one of the quantities, such as α_0, so as to form a new parameter $h_0/b\alpha_0$; however, this approach is inadequate when dealing with an aeroservoelastic problem. When considering the aeroelastic stability problem, the quantities of interest are $\omega_F b/V_F$, ω_R/ω_α, and $h_0/b\alpha_0$, where the subscript F refers to the value at flutter condition. To obtain these quantities, the model must have all other nondimensional parameters such as: $\bar{\mu}$, $(\omega_h/\omega_\alpha), \ldots$, etc., with the correct values. Furthermore, the external shape, i.e., airfoil type, and Reynolds number Re should also be maintained.

The model is subject to only three independent limitations, which are associated with the three primary quantities. The scaling for the primary quantities is expressed in general form by

$$\frac{L_m}{L_w} = n_L, \qquad \frac{T_m}{T_w} = n_T, \qquad \frac{M_m}{M_w} = n_M \qquad (5)$$

where the subscripts m and w refer to the model and full-scale configuration, respectively. Also note that another nondimensional parameter, namely, the nondimensional velocity $\bar{U} = (V/b\omega_\alpha$, also plays an important role when dealing with aeroelastic scaling. When compressibility is included in the aeroelastic scaling process the list of sixteen nondimensional parameters mentioned earlier, has to be augmented by two additional parameters: the Mach number M_∞ and the ratio of specific heats γ. Note that simultaneous scaling of Mach and Reynolds number is virtually impossible unless one uses the full-scale configuration.

The aeroelastic scaling considerations discussed above are based on classical flutter solutions obtained from Eqs. (1)-(3). Modern aeroelastic studies are usually based on refined computer simulations [15, 39]. Such computer solutions [17, 39] can be viewed as similarity solutions of the equations of motion governing the problem [1] and can be combined with the classical approach to obtain more general aeroelastic scaling requirements.

Recognizing that computer simulations can be used as similarity solutions to aeroelastic problems, enables one to develop modern or innovative scaling laws for aeroelastic or aeroservoelastic problems. Such scaling laws can be obtained from a two pronged approach, depicted in Fig. 2. First, basic aeroelastic similarity laws are obtained by pursuing the classical approach, for a typical cross section, described by Eqs. (1) - (4). From this approach a number of basic nondimensional parameters, which were discussed above, are identified.

In parallel a computer simulation for a specific aeroelastic or aeroservoelastic problem, which is under consideration, has to be developed [15]. Such computer simulations can produce quantities that are important for the more complex problem, such as: actuator forces or moments, hinge moments on control surfaces, power requirements for flutter suppression or vibration alleviation. Combining nondimensional values of these additional parameters, with the aeroelastic similarity parameters obtained from the classical approach, yields a more comprehensive set of aeroelastic scaling parameters. This new set of extended scaling requirements, represents a modern version of aeroelastic scaling laws.

To further illustrate this new approach, consider the aeroservoelastic problem associated with the system depicted in Fig. 1, where an active control system actuates the trailing edge flap which is used to suppress flutter. In this case it is important to determine scaling requirements for the hinge moment of the control surface during flutter suppression, together with its power requirements. The importance of scaling for these parameters is obvious, if one is interested in the practical implementation of such a controller on a full scale vehicle. Consider first the hinge moment per unit span

$$H = 2\rho V^2 b^2 C_h$$

and nondimensionalize it as

$$\begin{aligned}\bar{H} &= \frac{H}{m\omega^2 b^2} = \frac{2\rho V^2 b^2}{m\omega^2 b^2} C_h = \frac{2}{\pi}\left(\frac{\pi\rho b^2}{m}\right)\frac{V^2}{\omega^2 b^2} C_h \\ &= \frac{2}{\pi\mu}\frac{1}{k^2} C_h = \frac{2}{\pi}\frac{\bar{U}^2}{\mu}\left(\frac{\omega_\alpha}{\omega}\right)^2 C_h \qquad (6)\end{aligned}$$

An important quantity is the instantaneous power per unit span required for control flap actuation given by

$$P(t) = H(t)\dot{\beta}(t)$$

and the nondimensional instantaneous power per unit span that can be written as

$$\begin{aligned}\bar{P} &= \frac{P(t)}{m\omega^3 b^2} = \frac{2}{\pi}\left(\frac{\pi\rho b^2}{m}\right)\frac{1}{k^2} C_h \frac{\dot{\beta}}{\omega} \\ &= \frac{2}{\pi}\frac{\bar{U}^2}{\mu}\left(\frac{\omega_\alpha}{\omega}\right)^2 C_h \frac{\dot{\beta}}{\omega} = \frac{2}{\pi}\frac{\bar{U}^2}{\mu}\left(\frac{\omega_\alpha}{\omega}\right)^3 C_h \frac{\dot{\beta}}{\omega_\alpha} \qquad (7)\end{aligned}$$

For certain applications, instantaneous power can be misleading and therefore, it is useful to define an

average power; such a quantity, however, will be application dependent:

$$\bar{P}_{av} = \frac{2}{\mu}\frac{\bar{U}^2}{\mu}\left(\frac{\omega_\alpha}{\omega}\right)^3 \frac{1}{\bar{t}_2 - \bar{t}_1}\int_{\bar{t}_1}^{\bar{t}_2} C_h(\bar{t})\frac{\dot{\beta}}{\omega_\alpha}d\bar{t} \qquad (8)$$

The average power per unit span, given by Eq. (8), is the average power in a nondimensional time period $(\bar{t}_2 - \bar{t}_1)$, during which the pitch angle response is reduced by 50% from its initial value. Equations (6) - (8) have interesting implications when considering aeroservoelastic testing of aeroelastically scaled models and the application of these to a full-scale configuration.

2.1 ROTARY-WING AEROELASTIC SCALING CONSIDERATIONS

Next, the new approach, described in the previous section, for developing aeroelastic scaling laws for complex configurations involving active controls combined with adaptive materials based actuation is extended to rotary-wing applications.

It is possible to develop aeroelastic scaling considerations for rotary wing applications, similar to those developed for typical fixed-wing cross sections, by recognizing that the rotary-wing equivalent of a typical cross-section is the offset-hinged spring restrained blade model. Using appropriate springs this model, shown in Fig. 3, can be used to represent either an articulated blade or a hingeless blade. The equation of motion for such an offset hinged spring restrained blade can be taken from [52]. In Ref. 52 the equations of dynamic equilibrium for the blade configuration shown in Fig. 3, were derived for the fully coupled flap-lag-torsional dynamics of the blade, undergoing moderate deflections, in forward flight. The use of moderate blade deflections, introduces geometrically nonlinear terms in the structural, inertia and aerodynamic terms in the dynamic equations of equilibrium. The aerodynamic loads used in this study [52] are essentially quasi-steady aerodynamic loads corresponding to Greenberg's theory. Note that frequency domain aerodynamics are incompatible with forward flight and therefore the quasisteady assumption is required. Another alternative is the use of time domain aerodynamics, which is employed in Ref. 39.

Using the inertia, structural, aerodynamic and damping moments one can write the dynamic equations of equilibrium that can be used as the basis for formulating aeroelastic scaling laws for rotary-wing applications.

The inertia moments found in [52] are written as:

$$\begin{aligned} Q_{I_{x_3}} = \frac{m\Omega^2 R^3}{3}\Big[&\zeta\ddot{\beta} - \beta\zeta + \beta\ddot{\zeta} - 2(\beta\dot{\beta} + \zeta\dot{\zeta})\Big] \\ &+ \Omega^2\Big\{mx_I\cos\Theta_G\frac{R^2}{2}(\ddot{\beta} - \zeta\phi + \ddot{\zeta}\phi) + \\ &mx_I\sin\Theta_G\frac{R^2}{2}\big[-\zeta + \ddot{\zeta} + 2(\beta\dot{\beta} + \zeta\dot{\zeta}) + \phi\beta\big] \\ &+ \left(I_{MB_3}\cos^2\Theta_G + I_{MB_2}\sin^2\Theta_G\right) \\ &\left(-\ddot{\phi} + \ddot{\zeta}\beta + 2\dot{\beta}\dot{\zeta} + \zeta\ddot{\beta} - \ddot{\Theta}_G + \beta\zeta\right) \\ &+ \left(I_{MB_3}\sin^2\Theta_G + I_{MB_2}\cos^2\Theta_G\right) \\ &\left[\phi - \ddot{\phi} - 2\dot{\beta} + 2\dot{\phi}\zeta + 2\phi\dot{\zeta} + 2\zeta\dot{\Theta}_G - \Theta_G\right]\Big\} \end{aligned} \qquad (9)$$

$$Q_{I_{y_3}} = \frac{m\Omega^2 R^3}{3}(2\dot{\zeta}\beta - \ddot{\beta}) \qquad (10)$$

$$Q_{I_{z_3}} = \frac{m\Omega^2 R^3}{3}\left[\zeta - \ddot{\zeta} + 2(\zeta\dot{\zeta} + \beta\dot{\beta}) - \zeta(1 + 2\dot{\zeta})\right] \qquad (11)$$

The elastic restoring moments for an offset hinged spring restrained blade, with no hub and controls system flexibility, which is equivalent to a hingeless rotor blade, can be written as [52]

$$\begin{aligned} M_\beta = &(\beta - \phi\zeta)[K_\beta + (K_\zeta - K_\beta)\sin^2\Theta_G] + \\ &(\zeta + \phi\beta)(K_\zeta - K_\beta)\sin\Theta_G\cos\Theta_G \end{aligned} \qquad (12)$$

$$\begin{aligned} M_\zeta = &-(\zeta + \phi\beta)[K_\zeta - (K_\zeta - K_\beta)\sin^2\Theta_G] - \\ &(\beta - \phi\zeta)(K_\zeta - K_\beta)\sin\Theta_G\cos\Theta_G \end{aligned} \qquad (13)$$

$$M_\phi = -K_\phi(\phi - \zeta\beta) \qquad (14)$$

The aerodynamic moments can be written in a general form, that is more compact than the expressions in [52]

$$\begin{aligned} Q_{A_{x_3}} = \rho_A ab\Omega^2\frac{R^4}{4}f_{A_{x_3}}[&\zeta, \beta, \phi, \mu, x_A, \Theta_G, \\ &\cos\psi, \sin\psi, \lambda] \end{aligned} \qquad (15)$$

$$\begin{aligned} Q_{A_{y_3}} = -\rho_A ab\Omega^2\frac{R^4}{4}f_{A_{y_3}}[&\zeta, \beta, \phi, \mu, \Theta_G, \\ &\cos\psi, \sin\psi, \lambda] \end{aligned} \qquad (16)$$

$$\begin{aligned} Q_{A_{z_3}} = \rho_A ab\Omega^2\frac{R^4}{4}f_{A_{z_3}}[&\zeta, \beta, \phi, \mu, \Theta_G, \\ &\cos\psi, \sin\psi, \lambda, \frac{C_{d0}}{a}] \end{aligned} \qquad (17)$$

where $f_{A_{x_3}}$, $f_{A_{y_3}}$ and $f_{A_{z_3}}$ are complicated expressions given in Ref. 52. The structural damping moments can be expressed as:

$$Q_{D_{y_3}} = \Omega\dot{\beta}g_{SF} \qquad (18)$$

$$Q_{D_{z_3}} = -\Omega\dot{\zeta}g_{SL} \qquad (19)$$

$$Q_{D_{x_3}} = -\Omega\dot{\phi}g_{ST} \qquad (20)$$

Note, that when the blade has hinge offset e, and precone β_p the aerodynamic and inertia moments will also depend on these quantities.

The equations of equilibrium of the offset hinged spring restrained blade are given by

$$M_\beta + Q_{I_{y3}} + Q_{A_{y3}} + Q_{D_{y3}} = 0 \qquad (21)$$

$$M_\zeta + Q_{I_{z3}} + Q_{A_{z3}} + Q_{D_{z3}} = 0 \qquad (22)$$

$$M_\phi + Q_{I_{x3}} + Q_{A_{x3}} + Q_{D_{x3}} = 0 \qquad (23)$$

After substituting Eq. (9)-(20) into Eqs. (21)-(23), one obtains the dynamic equations of equilibrium for coupled flap-lag-torsional dynamics of the blade. The resulting dynamic equations of equilibrium are nonlinear, and for aeroelastic stability boundary calculations the equations have to be linearized about a static equilibrium position in hover, or a periodic equilibrium condition in the case of forward flight [18]. The equations provided above can be used as the basis for developing aeroelastic scaling laws in a manner similar to the classical scaling laws [6] described by Eqs. (1)-(4). More refined scaling laws can be obtained following the two pronged approach depicted in Fig. 2, where in addition to basic scaling laws, more refined laws for power consumption, and actuator forces and moments needed for active control applications can be obtained by using a suitable computer simulation. Refined simulations such as those described in Ref. 12, 39 and 40 can be employed to generate refined scaling laws for a variety of vibration reduction problems [12,40], including alleviation of blade vortex interaction induced vibration [12].

It is convenient to divide Eqs. (21)-(23) by $\Omega^2 I_b$, and introduce nondimensional quantities that are commonly used in helicopter rotor dynamics, such as $\gamma =$ Lock number $= 2\rho_A a b R^4/I_b$ where for a uniform blade $I_b = \frac{mR^3}{3}$ and define

$$\frac{K_{\beta B}}{\Omega^2 I_b} = \bar{\omega}_\beta^2 \quad ; \quad \frac{K_{\zeta B}}{\Omega^2 I_b} = \bar{\omega}_\zeta^2 \quad ; \quad \frac{K_\phi}{\Omega^2 I_b} = \frac{I_f}{I_b}\bar{\omega}_\phi^2$$

$$\frac{\Omega g_{SF}}{I_b \Omega^2} = \eta_{SF} 2\bar{\omega}_\beta \quad ; \quad \frac{\Omega g_{SL}}{I_b \Omega^2} = \eta_{SL} 2\bar{\omega}_\zeta$$

$$\frac{\Omega g_{ST}}{I_b \Omega^2} = \eta_{ST} 2\bar{\omega}_\phi$$

Rewriting the various parameters affecting the rotordynamic problem in terms of the three basic dimensions M, L, T (mass, length, time) and using dimensional analysis, it can be shown that the rotary-wing aeroelastic response problem is governed by several nondimensional parameters, that govern the solution, thus

$$\beta,\ \zeta,\ \phi \sim F_i\Big(M, Re, \mu, \frac{\bar{\omega}_\beta}{\bar{\omega}_\phi}, \frac{\bar{\omega}_\zeta}{\bar{\omega}_\phi}, \gamma, \frac{x_A}{R}, \frac{x_I}{R}, \frac{V^2}{gR}, \frac{E}{\rho_A V^2}, \lambda, \frac{C_{d0}}{a}, \frac{\omega b}{V}, \Theta_G, \eta_{Si}\Big) \qquad (24)$$

where $i = 1, 2, 3$ for flap, lag and torsion, respectively.

For complete similarity between dynamic behavior of the model and a full size configuration the function F_i must have the same values in each system, which implies that the nondimensional parameters in F_i must have the same value in both systems. Most of the parameters in Eq. (24) are self explanatory. A new parameter the *Froude number* $= \frac{V^2}{gR}$ appears if gravity loads on the blade are taken into account.

When comparing the parameters in Eq. (24) with those that govern the aeroelastic scaling of fixed wing problem treated in the previous section it is evident that these are more stringent, and satisfying all the relations simultaneously implies constructing a model that has the same dimensions as the full scale configuration.

The common practice in rotary-wing aeroelastic scaling has been to relax these stringent scaling requirements and build either a Mach scaled or Froude scaled model [26]. Furthermore, testing at full scale Re and M numbers is impossible, and usually model rotors are tested at Re numbers that are below full scale values.

It should be also mentioned that Froude scaling is important for aeroelastic stability testing in hover or forward flight, as well as for air and ground resonance aeromechanical testing. Mach scaled rotors are appropriate when testing vibration reduction using active control. However, it should be noted that hub shears and moments, can be also affected by the nonlinear steady state time dependent equilibrium position of the blade in forward flight, and Froude scaling can influence this equilibrium position.

As indicated earlier, the aeroelastic scaling laws described here, have to be combined with aeroelastic simulations [12, 39, 40], using the two pronged approach shown in Fig. 2, to generate refined scaling laws involving actuator power, and force and moment requirements, that are needed when using adaptive materials based actuation combined with active control for vibration reduction.

Finally, it is important to note that in many small scale tests, described in the next section of this paper, the difficulties associated with aeroelastic scaling have not been carefully addressed, and the models used have been very soft (or flexible) so as to accommodate the limited strain or force producing capability of the current generation of adaptive materials.

3 PROPERTIES OF ADAPTIVE MATERIALS

A simple introduction to smart structures and materials can be found in a recent book written by Culshaw [11]. The properties of the most important

types of adaptive materials being considered as candidates for potential aeroelastic applications are displayed in a convenient manner in Tables I and II. Table I displays the three primary types of materials, two different types of piezoelectric materials (PE), magnetostrictive materials (MS), and shape memory alloys (SMA), together with their strain producing capability, and concise comments regarding some of their basic characteristics and methods of actuation.

Table II presents additional information on characteristics that are relevant for various applications, such as: elastic constants, mass density, and the coupling or active characteristic coefficients that relate the input quantity (load, electric field, magnetic field or temperature) to the resulting strain.

Based on the information provided in Tables I and II one can conclude that shape memory alloys (SMA) produce large amounts of strain and force, however, the heating and cooling poses serious restrictions on frequency response and therefore are applicable to low frequency, or static aeroelastic applications. Piezoceramics, have excellent frequency response characteristics, however, currently serious limitations on their force and stroke producing capability exist. It is also important to note that the area of characterization of adaptive materials is still far from mature, and standard characterization tests are not available. These materials also often exhibit nonlinear and hysteretic behavior, and using these materials in the nonlinear regime can provide benefits that increase the limited strain producing capability present in these materials.

4 VIBRATION ALLEVIATION IN ROTORS USING CONTROLLED TRAILING EDGE DEVICES

The concept of using a trailing edge flap, similar to a Kaman servo flap, as a means for affecting the dynamic behavior of the rotor has been first considered by Lemnios and Smith [29]. Twenty years later, Millott and Friedmann have conducted a series of comprehensive studies [35–38] demonstrating that an actively controlled trailing edge flap (ACF), shown in Fig. 4, is capable of producing vibration reduction comparable to conventional individual blade control (IBC), where the blade is given a time varying pitch input, at its root, in the rotating system [19]. While the levels of oscillatory hub shear and moment vibration reduction obtained with the ACF were similar to those due to conventional IBC, the power requirements for the ACF were 10-20 times lower than those required for implementing conventional IBC. To emphasize the statements made illustrative results are presented for the case studied in [19, 38]. The actively controlled flap for this case was modeled as a 12% span, one fourth chord, trailing edge flap centered about 75% span position. Blade fundamental frequencies were given by $\omega_{F_1} = 1.124$; $\omega_{L_1} = 0.732$; and $2.5 \leq \omega_{T_1} \leq 5.0$, and the configuration was representative of a four bladed hingeless rotor, similar to a MBB BO-105 helicopter, except for the variation in torsional frequency.

The 4/rev oscillatory hub shear and hub moment reduction, achieved by an optimal combination of 2/rev, 3/rev, 4/rev and 5/rev control flap angle inputs, introduced in the rotating reference frame is shown in Fig. 5. Figure 5 also contains comparison with vibration reduction obtained with conventional IBC where a similar combination of harmonic pitch inputs is provided at the blade root. It is evident from the figure that both approaches produce very similar levels of vibrations reduction when the blade torsional frequency is $\omega_{T_1} = 3.5$.

The control power requirements associated with these two approaches are illustrated in Fig. 6, and it is evident that power requirements for implementing conventional IBC are an order of magnitude larger. These results were also confirmed by the research conducted by Milgram, Chopra and Straub [33, 34]. It is therefore not surprising that a considerable number of studies have been conducted on using trailing edge devices utilizing adaptive materials based actuation such as: (1) bimorphs [27, 48]; (2) trailing edge flap with piezo-induced bending-torsion coupled actuator [3, 4]; (3) trailing edge flap actuated by piezo stacks [7]; and (4) ACF utilizing magnetostrictive actuation [16, 37], and (5) ACF utilizing mesoscale actuators [14, 40, 55].

One of the earliest studies of adaptive materials applied to development of actuator for trailing edge flap used for vibration was reported by Spangler and Hall [48]. The geometry of the bimorph actuated trailing edge flap configuration is shown in Fig. 7. The piezoelectric bimorph, is a combination of an adaptive material based actuator combined with a deflection amplifying lever arrangement shown in Fig. 7, which provides a tradeoff between the magnitude of force provided by the device and its deflection. The bimorph is an adaptive material based actuator with a small depth to length ratio h/l (where h is the distance separating the two piezoelectric layers of actuating material with thickness t), formed by bonding two piezoelectric strain actuators together, so that one expands and the other contracts longitudinally causing the equivalent of a change in local bending slope.

In the flap actuator the beam is linked to the flap as shown in Fig. 7 with an effective lever arm of distance d. For small deflections the relation between the flap deflection and deflections of the piezoelectric

beam tip can be written as $\delta_F = w_T/d$ and using a considerable number of simplifying assumptions it is shown in [48] that

$$\delta_F = \sqrt{\frac{9(h/t)^2 Elt}{8[1+3(\frac{h}{t})^2]\rho_A U_d^2 b^2 C_{M_\beta}}} d_{31} e$$

where E is the modulus of elasticity of the piezoelectric, l is the length of the bimorph, t is the piezoelectric actuating material thickness, U_d is a design velocity where the flap is supposed to operate, C_{M_β} is a hinge moment coefficient, d_{31} is the strain per voltage field strength of the PE actuator material, and e is the actuating voltage strength. For the case considered in Ref. 48 a small scale wind tunnel test was conducted on a nonrotating configuration resembling a CH-47 helicopter rotor blade, and peak flap responses of 17^o were obtained.

It is relevant to note, that the authors have attempted to develop some basic aeroelastic scaling considerations so as to determine how the result would apply to a full scale blade configuration. However, these scaling considerations were based on fixed-wing concepts and they are not similar to the aeroelastic scaling relations described in the previous section of this paper.

In a subsequent study [23] improvements to the earlier bimorph actuated flap were described. This improved design was tested, again, in a nonrotating test, and flap deflection of 11.5^o were obtained, in still air. According to the scaling considerations developed, that do not appear to be compatible with rotary-wing aeroelastic scaling requirements, described in the previous section, the authors conclude that these deflections would correspond to 5^o, for the flap centered at 90% span location.

The ideas initially proposed in [48] were implemented in a comprehensive study recently completed by Fulton and Ormiston [20]. This study takes advantage of the bimorph configuration shown schematically in Fig. 8, in this case the amplification is built into the actuator such that the strains of the upper and lower piezoelectric layers cause a vertical deflection of the beam tip which is much larger than the total deformation of either PZT layer. The blocked force associated with the actuator is matched with the aerodynamic moment acting on the flap, using the mathematical model developed by Spangler and Hall [48].

In the configuration shown in Fig. 8 the PZT bimorph bender is cantilevered to the main spar of the blade. A lever arm of length d projects forward from the flap to engage the tip of the cantilever PZT beam to produce flap rotational motion schematically shown in Fig. 8. Denoting the deflection of the bimorph at the tip by w_T, the flap deflection can be approximated, within the framework of small deflections and linear theory by $\delta_F = w_T/d$. To ensure the largest possible flap deflection the particular configuration is optimized. In this process Euler-Bernoulli beam theory is used, together with an assumption of perfect bimorph bond. The aerodynamic load on the flap is approximated using quasi-static, two dimensional linear airfoil theory. The study revealed that for any PZT thickness an optimum lever arm exists that matches flap stiffness with aerodynamic stiffness.

The final design obtained is shown in Fig. 9 taken from [20], which shows the airfoil cross section, PZT bimorph bender beam and flap lever arm mechanism, in the top portion of the figure. The blade planform showing the fiberglass spar, the active flap section and the PZT actuator layout is shown in the lower portion of the figure. This design has a flap chord equal to 10% blade chord. The bimorph actuated flap is centered at 75%R location, and it extends over 12% of the blade span. The bimorph to flap width ratio was 0.54. The design velocity was 270 ft/sec. The target flap deflection was 5^o, for a piezoelectric actuation strain of $\Lambda = d_{31}e$, where $d_{31} = 7.09 \times 10^{-6}$ mil/V, and the excitation voltage is 90V. A maximum voltage of 156V could be used without fatiguing the PZT material.

The bimorph actuated flap were installed in a two bladed hingeless rotor, with a diameter of 7.5 ft and chord of 3.4 inches. The rotor was Mach scaled and had reduced torsional stiffness. The nominal operating speed was 760 RPM, which corresponds to a tip speed of 298 ft/sec. It is important to note that the rotor system was not a dynamically scaled to be representative of any particular full scale rotor system, however model dynamic characteristics were determined to be sufficiently representative of an actual system so as to allow the study of various aspects of the problem that are representative of full scale systems, as far as fundamental structural dynamic characteristics are encountered. It is also important to note that the model was not equipped with a closed loop control system, and all the excitations were applied in the open loop mode. The blade instrumentation was also limited, and it consisted of measurements of flap deflection and blade root bending and torsion moments. The blades were essentially uniform, untwisted, using a NACA 0012 airfoil, with chordwise mass and aerodynamic center located at 0.25 chord. The blade was made of composites. The design minimized mechanical loss due to aerodynamic hinge moment, pivot bearing friction, tennis raquet inertia effect, and friction in the linkage mechanism.

The electrical excitation consisted of an AC voltage < 110 Vrms. The AC voltage was superimposed on a DC voltage used to bias the bimorph layers in the di-

rection of their polarization, to avoid depolarization by the relatively large AC voltage. Electrical power was provided through slip-rings. It is interesting to note that the two blades exhibited somewhat different characteristics, thought to be related to bimorph actuation effectiveness and structural and aerodynamic characteristics. At the operating speed (760 RPM) $\omega_{F_1} = 1.11/rev$; $\omega_{L_1} = 1.08/rev$, $\omega_{F_2} > 3/rev$, $\omega_{T_1} = 4.6/rev$. all the tests were carried out in hover, with $\theta_0 = 3.5^o$ in most cases.

Several interesting results from this comprehensive study are briefly reviewed here since they are indicative of the actual problems encountered during the practical implementation of adaptive material based actuation in a representative helicopter rotor. Figure 10 taken from [20], illustrates the nonlinear behavior of the PZT material under static, nonrotating conditions. The figure shows steady state flap deflections for a complete cycle of increasing and decreasing excitation voltage showing a characteristic hysteresis loop. This nonlinear characteristic is also evident under rotating conditions. Figure 11 shows the flap deflections versus excitation voltage for a 5 Hz excitation at 760 RPM, and a collective pitch of $\theta_0 = 3.5°$. The "dead band" region is evident at low excitation voltage due to PZT hysteresis noted from Fig. 10, however it is less pronounced than in the nonrotating case.

Subsequently the dynamic tests conducted in this study were aimed at determining the aerodynamic pitch and lift loads that could be produced by flap actuation. Under certain conditions flap control reversal was encountered and explained using a simple analytical model. Frequency response functions (FRF) of the blade flapping moment, and torsion moment to elevon deflection input were obtained at the nominal operating speed and a limited number of lower values of RPM. The frequency response functions obtained for blade root flap bending response due to flap motion available imply that it will be possible to demonstrate significant reductions of the 3, 4 and 5/rev vibratory bending moments in forward flight in future tests.

It should be also noted that significant differences in flap performance, and torsion and bending moment responses between the two blades were evident from the measured results. However, it is felt that these blade to blade differences will not have a major impact on the planned exploratory investigations in forward flight.

Another study describing the testing and validation of a Froude scaled helicopter rotor model with piezo-bimorph actuated trailing edge flaps has been recently published by Koratkar and Chopra [27]. This study describes the development and testing of a two bladed hingeless rotor with carefully designed, four layered piezo-bimorph actuators. The rotor diameter was 6 ft, blade length was 26 inches, blade chord was 3 inches and nominal operating speed was 900 RPM. The integral flap, was 20% of blade chord, and it was centered at 90% span, and extended over 4% of the blade radius. The 1.5 inch span flap was driven by a one inch wide four layered piezo-bimorph actuator, operated at 95 Vrms. The rotor was tested in hover, at a tip Mach number of M=0.245. At a 15 Hz excitation frequency and nominal operating speed flap deflections of $\pm 4^o$ were achieved. When the frequency of excitation was increased to 60 Hz, 4/rev, $\pm 6^o$ flap deflections were obtained.

The authors recognized that Froude scaled rotors are required primarily for aeromechanical stability testing and that for vibration reduction studies a Mach scaled rotor is preferable. Therefore the last part of the paper is devoted to the preliminary design of a Mach scaled rotor, on which a larger flap actuated by two bimorphs will be used for vibration reduction.

A completely different approach for piezoceramic actuation of a trailing edge control surface has been described in a series of papers written by Bernhard and Chopra [3–5]. In this configuration the empty space available in the spar is utilized to lay-up a long beam with alternating composite lay-up excited by surface bonded piezoceramic elements, schematically shown in Fig. 12. By alternating the lay-up directions of bending-torsion coupling producing laminates, from section to section, along the length of the composite beam, and alternating the polarity of the piezoelectric layers as well, it is possible to have cancellation of the induced bending curvatures, while torsion is added from segment to segment. A disadvantage of this configuration is that the outboard bearing is loaded by the moment due to centrifugal forces acting on the flap [3, 4]. In the most recent version of this concept [5] this potential difficulty was eliminated by replacing the trailing edge flap by a swiveling tip, denoted by the term smart active blade tip (SABT).

This concept is currently being implemented in a four bladed bearingless rotor with diameter of 1.8 m, a nominal operating speed of 900 RPM and a NACA 0012 airfoil with a 76.2 mm chord. The rotor is Mach scaled. The active tip extends over 10% of blade span. While this concept hold promise, its control characteristics are highly localized (at the blade tip), and its ability to reduce vibrations remains to be determined.

Finally it should be mentioned that this model rotor configuration is identified as a 1/8 scale model. The information provided in the papers describing the configuration provides very limited data on the

design, thus one can not determine what is the degree of aeroelastic scaling enforced for the model.

Another alternative to the piezo-bimorph, and piezo-induced bending torsion actuation approaches is a straightforward piezo stack actuation device. In such a device a large number of piezoelements are bonded together by means of a coupling adhesive [7]. The displacement of the device in the direction normal to its plane is given by

$$\delta_S = nd_{33}(V/t)$$

where δ_S is the displacement, n-is number of piezoelements, V is the applied voltage and t is the thickness of piezo element layer and d_{33} is the piezoelectric constant. It should be noted that δ_S increases with the number of piezoceramic sheets contained in the stack. Integrating the stack with a mechanical lever produces further amplification of the displacements.

The practical implementation of a piezo-stack actuator for an actively controlled flap on the MD-900 Explorer rotor was studied by Straub and Hassan [50]. This fairly sophisticated system is being currently implemented on an actual bearingless rotor system. An interesting aspect of this system is that an aerodynamic tab is used as an aerodynamic amplification device to enhance the moment produced by the piezostack, and improve its performance using an "aerodynamic lever".

It is important to mention that concept of using the energy from the airstream to reduce the force/deflection requirements of adaptive materials based actuation has been also explored by Loewy [32]. In this innovative approach the marginally stable, actively controlled flap is used so that it extracts energy from the flow, and thus it amplifies significantly the force/deflection producing capability of the adaptive materials based actuation.

It is evident from review of the research aimed at developing trailing edge control devices, using adaptive materials based actuators, that this concept has received considerable attention due to its potential for vibration reduction in helicopters. The principal advantages of this concept are: (1) low power requirement; (2) versatility, two or more ACF devices can be distributed along the blade span [40], and these can address different objectives, such as vibration reduction combined with performance enhancement, this statement applies to all the configurations considered except SABT; (3) minimal effect on the helicopter airworthiness, since the primary control of the helicopter is still accomplished through a conventional swashplate.

However, it should be emphasized that rotary-wing aeroelastic scaling requirements have not been carefully implemented for the few ACF that have been experimentally tested, and therefore the issue of its implementation on a full scale configuration still remains to be answered by conducting an appropriate test.

5 VIBRATION REDUCTION IN HELICOPTER ROTORS USING THE ACTIVE TWIST ROTOR (ATR)

An alternative to the vibration reduction approach based on ACF with, adaptive materials based actuation, is to twist the entire rotor by embedding adaptive materials into the rotor itself or by bonding piezoelectric patches to the surface of the blade. In this case a time dependent distributed twist over the length of the entire blade can be used in a manner that resembles individual blade control (IBC). However, it should be noted that conventional IBC implies that the time dependent pitch input is provided at the root of the blade in the rotating system [19].

One of the most comprehensive studies in this area was carried out by Chen and Chopra [8,9] who developed a 1/8 Froude scaled, 6 ft diameter, two bladed bearingless rotor model, with a NACA 0012 airfoil and a chord of 3 inches. Banks of piezoelectric torsional actuators capable of manipulating blade twist at harmonics of the rotational speed were used. The piezoceramic actuators were embedded under the fiberglass blade skin in banks of discrete actuators at angles of $\pm 45°$ on the top and bottom surfaces respectively. The actuators were 2.0 inches long and 0.25 inch wide, to minimize transverse actuation. A number of different blade configurations were built and tested. The maximum twist response at the blade tip was of order 0.5°, at 900 RPM with dual layer actuators. Unfortunately, for viable control applications a tip twist of 1°-2° is required.

Another active twist rotor was developed almost by coincidence using the piezo-induced bending-torsion coupled beam discussed earlier [5] and clamping it at the tip. By locking the outboard end of the actuator beam in a rib at the end of the blade, the actuator tends to twist the entire blade. Only a limited number of hover tests were conducted and the maximum tip twist was approximately 0.5°. Thus it appears that this configuration is not significantly better than that developed earlier by Chen and Chopra [9], except that it is simpler, was developed faster, and at a lower cost.

A different approach is the integral twist-actuated rotor blade developed jointly by MIT and Boeing [43] and [13]. The integral twist is introduced by embedding anisotropic active plies within the composite spar of the blade to induce shear stresses which create the twist shown in Fig. 13. The active plies are a piezoelectric fiber composite (PFC), which is a

composite actuator that was developed for embedding within composite laminates. The actuator consists of continuous aligned electroceramic fibers in an epoxy-based matrix which is sandwiched between two layers of polymid film. The performance of PFC system is improved by using an Interdigitated Electrode (IDE) pattern, shown in Fig. 14, which orients the applied field along the active fibers, enabling the use of primary piezoelectric.

Initially this approach was tested on a proof concept configuration consisting of a 1/16 scale CH-47 helicopter blade and tip twist angles of 1.4° were obtained with 2000 volts of applied excitation, on a blade which had a 50% reduction in its torsional stiffness [13]. Furthermore, the test was conducted on a nonrotating blade and the model was Froude scaled, for no obvious reason, since the goal was vibration reduction. Reference 9 also presents a detailed preliminary design type analysis of such a CH-47 actively twisted blade, employing several questionable assumptions. A number of conclusions on issues such as vibration reduction, performance enhancement, and power requirements on the controllable twist rotor are presented. These conclusions appear to be somewhat optimistic. The design of a 1/6 Mach scaled CH-47 blade is also discussed and there is no attempt to deal with aeroelastic scaling issues.

In Ref. [43] a segment of 1/6 Mach scaled blade was tested in a static nonrotating test. The length of this segment was 0.6 feet and half of its length was active. The configuration corresponds to a CH-47 blade with torsional stiffness reduced by 50%. The results of this test are shown in Fig. 15, taken from [43] where the twist rate is plotted as a function of applied voltage. It is interesting to note again the hysteretic nature of piezo actuation. It is also noteworthy that the twist obtained in this test was approximately 50% lower than the predicted twist.

It is relevant to compare the concept of actively twisted rotor with ACF, when applied to vibration reduction of rotors in forward flight. As indicated in Fig. 6 of this paper, the power requirements of conventional IBC are an order of magnitude (and sometimes more) higher than those of the ACF for comparable amounts of vibration reduction. It should be emphasized that in the conventional IBC context the blade is given a pitch input at its root, and it undergoes rigid body rotation about its feathering axis. For the actively twisted rotor the desired pitch at the blade tip is $\approx 2°$, and it is obtained by elastically twisting the entire blade, which causes further increases in power requirement, possibly by a factor of three or more, since considerable strain energy is needed to deform a long structural member, such as a rotor blade.

Furthermore, actively controlled trailing edge devices can be segmented, and used and controlled independently of each other [40], for vibration reduction as well as other purposes, such as performance enhancement or noise reduction. Local control, obtained at spanwise location, with the actively twisted rotor is very difficult. Thus it appears that the actively twisted rotor does with great difficulty, what the ACF does easily. The comparison between these two approaches seems to clearly indicate the superiority of the ACF as a means for rotor vibration control.

6 CONCLUDING REMARKS

A novel two pronged approach is presented for obtaining aeroelastic and aeroservoelastic scaling laws in the framework of modern aeroelasticity. The approach consists of parallel combinations of classical aeroelastic scaling laws with sophisticated computer simulation, that play the role of similarity solutions, to yield refined scaling laws. This scaling laws provide information on hinge moments, actuator forces, and power requirements, which play an important role in aeroservoelastic applications.

It is shown that rotary-wing aeroelastic laws, can be obtained in a manner resembling fixed-wing aeroelastic scaling based on a typical cross section by recognizing that the offset hinged spring restrained blade model is the rotary-wing equivalent of a typical cross section.

Aeroelastic scaling of rotary-wing problems is more complicated than its fixed wing counterpart. Thus, one has to use relaxed requirements which imply that rotors have to be either Mach scaled or Froude scaled. Mach scaling is suitable for simulating vibration reduction studies, while Froude scaling is recommended for aeromechanical stability problems.

The problem of vibration reduction in helicopter rotors using adaptive materials and its scaling is addressed using the scaling requirements developed. The role of small scaled models used in feasibility studies aimed at vibration reduction using adaptive materials based actuation is examined. It is noted that the current generation of adaptive materials have force and stroke producing limitations, and therefore feasibility tests of such actuators, are often performed on small scale model that are quite flexible, and are not aeroelastically scaled.

The aeroelastic scaling considerations presented in the paper indicate that in many cases extrapolation of results obtained to the full scale configuration is difficult, and sometimes impossible.

Based on the evidence available to date it appears that the ACF seems to be substantially more suitable for vibration reduction applications that the actively

twisted rotor.

7 ACKNOWLEDGMENTS

This research supported in part by the U.S. Army, Research office under grant DAA 04-95-1-0095 with Dr. J. Prater as grant monitor. This research was inspired by AFOSR grant F49620-94-1-0400 which supported the development of aeroelastic scaling laws for fixed wing vehicles. The author is indebted to Major Brian Sanders, Ph. D. who was the grant monitor, and strongly encouraged the author to pursue this research.

References

[1] Baker, W. E., Westine, P. S., and Dodge, F. T., *Similarity Methods in Engineering Dynamics: Theory and Practice of Scale Modeling*, Elsevier, Revised Edition, 1991.

[2] Barenblatt, G. I., *Scaling, Self-similarity, and Intermediate Asymptotics*, Cambridge University Press, 1996.

[3] Bernhard, A.F., and Chopra, I., "Development and Hover Testing of a Smart Trailing Edge Flap with Piezo-Induced Bending-Torsion Coupled Actuation," *AHS National Technical Specialists Meeting on Rotorcraft Structures*, Williamsburg, VA, Oct. 30 – Nov. 2 1995.

[4] Bernhard, A.P.F., and Chopra, I., "Development of a Smart Moving Blade Tip Activated by a Piezo-Induced Bending-Torsion Coupled Beam," *SPIE Conference on Smart Structures and Integrated Systems*, San Diego, CA, Feb. 26-29, 1996, pp. 19 – 35.

[5] Bernhard, A.P.F., and Chopra, I., "Development of a Smart Moving-Blade-Tip and an Active-Twist Rotor Blade Driven by Piezo-Induced Bending-Torsion Coupled Beam," *53rd Annual Forum of the American Helicopter Society*, Virginia Beach, VA., April 29 - May 1 1997.

[6] Bisplinghoff, R.L., Ashley, H., and Halfman, R.L., *Aeroelasticity*, Addison-Wesley, 1955.

[7] Chandra, R., and Chopra, I., "Actuation of Trailing Edge Flap in a Wing Model Using Piezostack Device," in *Proceedings of the 38th AIAA/ASME/ASCE/AHS/ASC Structures, Structural Dynamics and Materials Conference*, Kissimmee, FL, April 7-10 1997.

[8] Chen, P.C., and Chopra, I., "Induced Strain Actuation of Composite Beams and Rotor Blades with Embedded Piezoceramic Elements," *Smart Materials and Structures*, Vol. 5, No. 1, Feb. 1996, pp. 35 – 48.

[9] Chen, P.C., and Chopra, I., "Development of a Smart Rotor Blade with Induced Strain Actuation of Blade Twist," *AIAA Journal*, Vol. 35, No. 1, Jan. 1997, pp. 6 – 16.

[10] Chopra, I., "Status of Application of Smart Structures Technology to Rotorcraft Systems," *Proceedings of Innovation in Rotorcraft Technology*, London, UK, Royal Aeronautical Society, June. 24-25 1997, pp. 13.1 – 13.24.

[11] Culshaw, B., *Smart Structures and Materials*, Boston/London, Artech House, 1996.

[12] de Terlizzi, M., and Friedmann, P.P., "Aeroelastic Response of Swept Tip Rotors Including the Effects of BVI," *Proceedings of the 54th Annual Forum of the American Helicopter Society*, Washington, DC, May, 20-22 1998.

[13] Derham, R.C., and Hagood, N.W., "Rotor Design Using Smart Materials to Actively Twist Blades," *52nd Annuual Forum of the American Helicopter Society*, Washington, DC, June 4-6 1996, pp. 1242 – 1252.

[14] Friedmann, P. P., "The Promise of Adaptive Materials for Alleviating Aeroelastic Problems and Some Concerns," *Proceedings of Innovation in Rotorcraft Technology*, London, UK, Royal Aeronautical Society, June 24-25 1997, pp. 10.1 – 10.16.

[15] Friedmann, P. P., Guillot, D., and Presente, E. H., "Adaptive Control of Aeroelastic Instabilities in Transonic Flow and its Scaling," *Journal of Guidance, Control, and Dynamics*, Vol. 20, No. 6, Nov. - Dec., 1997, pp. 1190 – 1199.

[16] Friedmann, P.P., Carman, G.P., and Millott, T.A., "Magnetostrictively Actuated Control Flaps for Vibration Reduction in Helicopter Rotors - Design Considerations for Implementation," *Proceedings of the 36th Israel Annual Conference on Aerospace Sciences*, Tel-Aviv/Haifa, Israel, February 1996, pp. 295 – 306.

[17] Friedmann, P.P., Guillott, D., and Presente, E.H., "Adaptive Control of Aeroelastic Instabilities in Transonic Flow and Its Scaling," AIAA Paper 97-0551, *35th Aerospace Sciences Meeting and Exhibit*, Reno, NV, January 6-10 1997.

[18] Friedmann, P.P., and Hodges, D.A., "Rotary-Wing Aeroelasticity with Application to VTOL Vehicles," *Flight Vehicles, Materials, Structures, and Dynamics-Assessment and Future Directions*, Noor, A.K. and Venneri, S.L., Eds., Vol. 5, New York, ASME, 1993, Ch. 6, pp. 299 – 391.

[19] Friedmann, P.P., and Millott, T.A., "Vibration Reduction in Rotorcraft Using Active Control: A Comparison of Various Approaches," *AIAA Journal of Guidance, Control and Dynamics*, Vol. 18, No. 4, July-August 1995, pp. 664 – 673.

[20] Fulton, M.V., and Ormiston, R.A., "Hover Testing of a Small-Scale Rotor with on-Blade Elevons," *53rd Annual Forum of the American Helicopter Society*, Virginia Beach, VA., April 29 - May 1 1997.

[21] Gade, P.V.N., and Inman, D.J., "Controller Design for Wing/Store Flutter Suppression of an Airfoil in Incompressible Flow," AIAA Paper 96-1633, *Proceedings 37th AIAA/ASME/ASCE/AHS/ACS Structures, Structural Dynamics and Materials Conference*, Salt Lake City, UT, April 1996, pp. 221 – 229.

[22] Giurguitiu, V., Chaudhry, Z., and Rogers, C.A., "Active Control of Helicopter Rotor Blades with Induced Strain Actuators," AIAA Paper 94-1765, *AIAA/ASME Adaptive Structures Forum*, Hilton Head, SC, April 1994, pp. 228 – 297.

[23] Hall, S.R., and Prechtl, E.F., "Development of a Piezoelectric Servoflap for Helicopter Rotor Control," *Smart Materials and Structures*, Vol. 5, No. 1, February 1996, pp. 26 – 34.

[24] Heeg, J., "Analytical and Experimental Investigation of Flutter Suppression by Piezoelectric Actuation," NASA, TP 3241, February 1993.

[25] Heeg, J., Scott, C., and McGowan, A., "Aeroelastic Research: Using Smart Structures Concepts," *Aeroelasticity and Fluid Structure Interaction Problems*, Friedmann, P.P., and Chang, J.C.I., Eds., Vol. AD-44, Chicago, IL, ASME, November 6-11 1994, pp. 161 – 173.

[26] Hunt, G. K., "Similarity Requirements for Aeroelastic Models of Helicopter Rotors," Aeronautical Research Council Current Papers CP No. 1245, London, UK, January 1973.

[27] Koratkar, N.A., and Chopra, I., "Testing and Validation of a Froude Scaled Helicopter Rotor Model with Piezo-Bimorph Actuated Trailing Edge Flaps," in *SPIE Smart Structures and Materials Symposium*, San Diego, CA, March 2-6 1997.

[28] Lazarus, K., Crawley, E., and Lin, C., "Fundamental Mechanism of Aeroelastic Control with Control Surface and Strain Actuation," *Journal of Guidance, Control and Dynamics*, Vol. 18, No. 1, Jan. 1995, pp. 10 – 17.

[29] Lemnios, A.Z., and Smith, A.F., "An Analytical Evaluation of the Controllable Twist Rotor Performance and Dynamic Behavior," Kaman, TR R-794, 1972.

[30] Lin, C.Y., Crawley, E.F., and Heeg, J., "Open and Closed-Loop Results of a Strain Actuated Active Aeroelastic Wing," *Journal of Aircraft*, Vol. 33, No. 5, Sep.-Oct. 1996, pp. 987 – 994.

[31] Loewy, R.G., "Recent Developments in Smart Structures with Aeronautical Applications," *Proceedings of the Israel Conference on Aerospace Sciences*, February 1997.

[32] Loewy, R.G., and Tseng, S.P., "Tests of an Unstable Lifting Surface Stabilized by a Simulated Smart Structure," in *6th ARO International Workshop on Dynamics and Aeroelastic Stability Modeling of Rotorcraft Systems*, University of California, Los Angeles, CA, November 8-10 1995.

[33] Milgram, J., "A Comprehensive Aeroelastic Analysis of Helicopter Main Rotors with Trailing Edge Flaps for Vibration Reduction," Ph.D. Dissertation, University of Maryland, Dept. of Aeronspace Engineering, College Park, MD, January 1997.

[34] Milgram, J., Chopra, I., and Straub, F.K., "A Comprehensive Rotorcraft Aeroelastic Analysis with Trailing Edge Flap Model: Validation with Experimental Data," *52nd Annual Forum of the American Helicopter Society*, Washington, DC, June 4-6 1996, pp. 715 – 725.

[35] Millott, T., and Friedmann, P.P., "The Practical Implementation of an Actively Controlled Flap to Reduce Vibrations in Helicopter Rotors," *Proceedings of the 49th Annual Forum of the American Helicopter Society*, St. Louis, MO, may 1993, pp. 1079 – 1092.

[36] Millott, T.A., and Friedmann, P.P., "Vibration Reduction in Helicopter Rotors Using an Active Control Surface Located on the Blade," AIAA Paper 92-2451, *Proceedings of 33rd Structures, Structural Dynamics, and Materials Conference*, Dallas, TX, April 1992, pp. 1974 – 1988.

[37] Millott, T.A., and Friedmann, P.P., "Vibration and Reduction in Hingeless Rotor Using an Actively Controlled Trailing Edge Flap: Implementation and Time Domain Simulation," AIAA Paper 94-1306, *Proceedings of 35th AIAA/ASME/ASCE/AHS/ASC Structures, Structual Dynamics and Materials Conference*, Hilton Head, SC, April 18-20 1994, pp. 9 – 22.

[38] Millott, T.A., and Friedmann, P.P., "Vibration Reduction in Helicopter Rotors Using an Actively Controlled Partial Span Trailing Edge Flap Located on the Blade," NASA, CR 4611, June 1994.

[39] Myrtle, T.F., and Friedmann, P.P., "Unsteady Compressible Aerodynamics of a Flapped Airfoil with Application to Helicopter Vibration Reduction," AIAA Paper 97-1083-CP, *Proceedings of the 38th AIAA/ASME/ASCE/AHS Structures, Structural Dynamics and Materials Conference*, Kissimmee, FL, April, 7-10 1997, pp. 224 – 240.

[40] Myrtle, T.F., and Friedmann, P.P., "Vibration Reduction in Rotorcraft Using the Actively Controlled Trailing Edge Flap and Issues Related to Practical Implementation," *Proceedings of the 54th Annual Forum of the American Helicopter Society*, Washington, DC, May, 20-22 1998.

[41] Presente, E. H., and Friedmann, P. P., "Aeroservoelasticity in Compressible Flow and Aeroelastic Scaling Considerations," *Proceedings of the 4th International Symposium on Fluid-Structure Interactions, Aeroelasticity, Flow-Induced Vibration and Noise*, Vol. III, (P.P.Friedmann and M.P. Paidoussis, Editors) AD-Vol. 53-3, Dallas, TX, November 16 - 21 1997, pp. 105 – 119.

[42] Regier, R.A., "The Use of Scaled Dynamic Models in Several Aerospace Vehicle Studies," *Proceedings of ASME Colloquim on Use of Models and Scaling in Shock and Vibration, Philadelphia, PA*, Winter Annual Meeting of ASME Philadelphia, PA, published by ASME, New York, 1963, pp. 34 – 50.

[43] Rodgers, J.P., Hagood, N.W., and Weems, D.B., "Design and Manufacture of an Integral Twist-Actuated Rotor Blade," AIAA Paper 97-1264, *Proceedings of the 38th AIAA/ASME/ASCE/AHS/ASC Structures, Structural Dynamics and Materials Conference*, Kissimmee, FL, April 7-10 1997.

[44] Scott, R.C., "Control of Flutter using Adaptive Materials," Master's Thesis, School of Aeronautics and Astronautics, Purdue University, West Lafayette, IN, 1990.

[45] Scott, R.C., and Weisshaar, T.A., "Controlling Panel Flutter Using Adaptive Materials," *Proceedings of 32nd AIAA/ASME/ASCE/AHS/ACS Structures, Structural Dynamics, and Materials Conference*, Baltimore, MD, 1991.

[46] Scruton, C. and Lambourne, N.C., "Similarity Requirements for Flutter Model Testing," *AGARD Manual on Aeroelasticity*, Vol. IV, Ch. 6, New York, NATO, 1963.

[47] Song, O., Librescu, L., and Rogers, C.A., "Static Aeroelasticity Behavior of Adaptive Aircraft Wing Structures Modelled as Composite Thin-Walled Beams," *International Forum on Aeroelasticity and Structural Dynamics*, Aachen, Germany, 1991.

[48] Spangler, R.L., and Hall, S., "Piezoelectric Actuators for Helicopter Rotor Control," AIAA Paper 90-1076 CP, *Proceedings 31st AIAA/ASME/ASCE/AHS/ACS Structures, Structural Dynamics, and Materials Conference*, Long Beach, CA, April 1990, pp. 1589 – 1599.

[49] Straub, F.K., "Smart Materials Actuation in Rotor Technology," USA ATCOM, TR 94-D-10, December 1975.

[50] Straub, F.K., and Hassan, A., "Aeromechanic Considerations in the Design of a Rotor with Smart Material Actuated Trailing Edge Flaps," *52nd Annuual Forum of the American Helicopter Society*, Washington, DC, June 4-6 1996, pp. 704 – 714.

[51] Theodorsen, T., and Garrick, I. E., "Nonstationary Flow About a Wing-Aileron-Tab Combination Including Aerodynamic Balance," NACA, TR 736, May 1942.

[52] Venkatesan, C., and Friedmann, P.P., "Aeroelastic Effects in Multi-Rotor Vehicles with Applications to a Hybrid Heavy Lift System, Part I: Formulation of Equations of Motion," NASA, CR 3822, August 1984.

[53] Weisshaar, T.A., "Aeroservoelastic Control Concepts with Active Materials," *Aeroelasticity and Fluid Structure Interaction Problems*, Friedmann, P.P. and Chang, J.C.I., Eds., Vol. AD-44, Chicago, IL, ASME, November 6-11 1994, pp. 125 – 146.

[54] Weisshaar, T.A., and Ehlers, S.M., *Adaptive Aeroelastic Composite Wings-Control and Optimization Issues* in *Composites Engineering*, Vol. 2, Pergamon Press, 1992, pp. 457 – 476.

[55] Zhu, J., Wang, D., Kim, C.J., and Carman, G.P., "Development of Mesoscale Actuation Device," *Proceedings of ASME Aerospace Division, AD Vol. 52, ASME International Mechanical Engineering Conference and Exhibit*, Atlanta, GA, November 1996, pp. 649 – 654.

TABLE 1: USEFUL PROPERTIES OF ACTIVE MATERIALS

Material	Manufacturer's Designation (TM's)	Actuation Principle & Max. Strain Capability	Comments
Ceramic (Lead Zirconate-Lead Titanate)	PZT	Piezoelectric (PE) 600 - 1000μ	• Active Characteristics Induced by "poling"; i.e., applying an electric field, typically ~2500 v/mm. • High Frequency Capability • Max Excitation Field ~2000 v/mm
Polymer (Polyvinylidine Fluoride)	PVDF	Piezoelectric (PE) 150μ	• Induced Strain Very Different in Two Directions
Rare Earth Elements Alloyed with Iron	Terfenol Samfenol	Magnetostrictive (MS) 1400 - 2000μ	• Requires Compressive Prestress and Magnetic Field Generating coils and Flux Guidance Material • High Frequency Capability, but with Reduced Amplitudes as Frequency Increases • Max. Induced Strain ~2000μ
Nickel Titinate, NiTi (or Compounds with Copper, or Aluminum; NiTiCu or CuAlNi)	Nitinol Flexinol	Shape Memory Alloy 4000 - 5000μ	• Actuation Requires Heating and Cooling; Unless Special Cooling is Provided, Cycling Probably Restricted to <5HZ. • Material Behavior is Highly Nonlinear (i.e., "Bang-Bang") • Max Induced Stress 20 x 10^3 (psi)

TABLE 2: CHARACTERISTICS OF ACTIVE MATERIALS

Manufacturer's Designation (TM's)	E Young's Modulus	Mass Density	Stress Free Coupling Factor (Active Characteristic)
PZT	8.8 10^6 (psi) 60.6 (GPa)	0.97-1.55 × 10 $\left(\frac{\text{slugs}}{\text{ft}^3}\right)$ 5-8 × 10^3 (kg/m^3)	d^*_{31} = 165 × 10^{-9} $\left(\frac{\text{mm}}{\text{v}}\right)$ d_{33} = 3.8-15. 10^{-9} $\left(\frac{\text{mm}}{\text{v}}\right)$
PVDF	0.29 × 10^6 (psi) 2.0 (GPa)	3.49 × 10 $\left(\frac{\text{slugs}}{\text{ft}^3}\right)$ 1.8 × 10^3 (kg/m^3)	d_{31}= 23. × 10^{-9} $\left(\frac{\text{mm}}{\text{v}}\right)$
Terfenol Samfenol	5 × 10^6 (psi) 35. (GPa)	1.8 × 10 $\left(\frac{\text{slugs}}{\text{ft}^3}\right)$ 9.25 × 10^3 (kg/m^3)	0.8 $\left(\frac{\mu}{Oe^{**}}\right)$
Nitinol Flexinol	3.6-9.7 × 10^6 (psi) 25. -67 × (GPa)	1.29 × 10 $\left(\frac{\text{slugs}}{\text{ft}^3}\right)$ 6.6 × 10^3 (kg/m^3)	10.4 $\frac{BTU}{\#}$ (Heat of Transformation)

* Coupling factors, d_{ij} depend on direction of "poling" axis and voltage excitation direction; i = j implies poling axis, excitation direction and resulting strain are all in same direction; i ≠ j implies poling and excitation axis are normal to each other, shearing strain about a third normal axis results.

** Oersteds

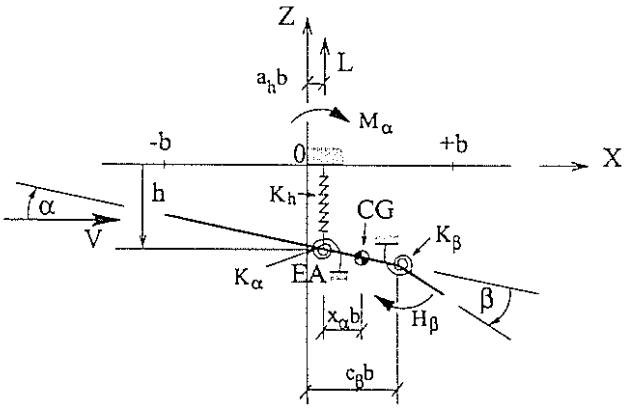

Figure 1: Definition of parameters for three degree of freedom aeroservoelastic model

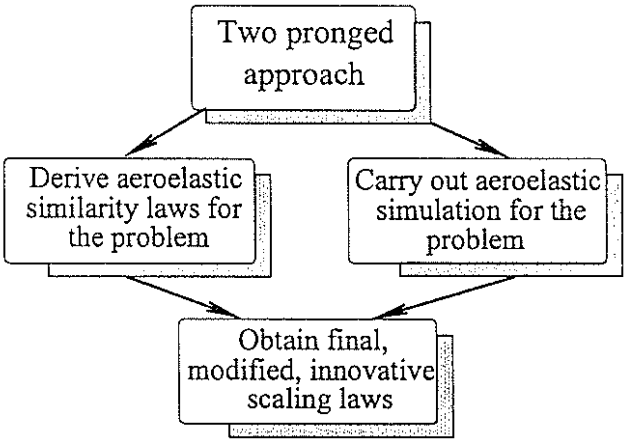

Figure 2: Two pronged approach to generating refined aeroelastic scaling laws

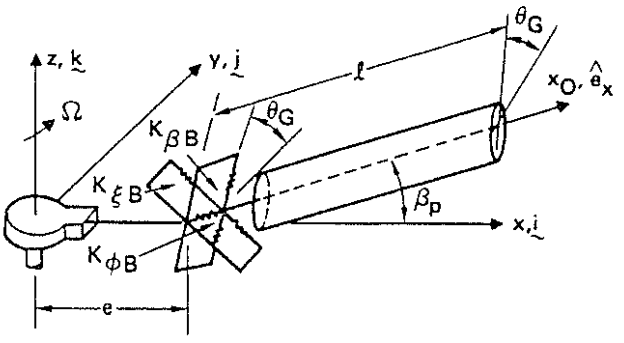

Figure 3: Offset hinged spring restrained blade model of a hingeless blade

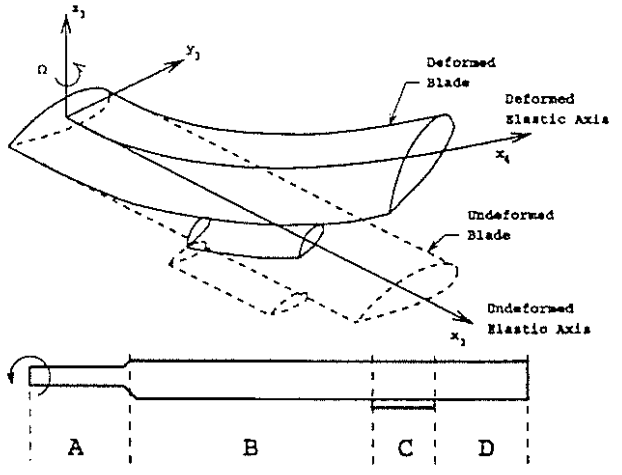

Figure 4: Blade model with partial span, actively controlled, trailing edge flap

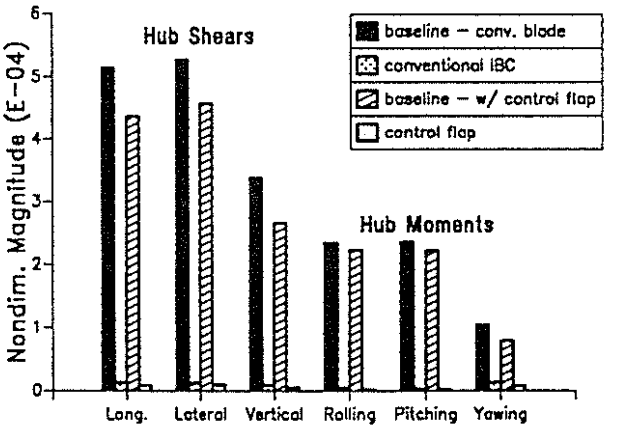

Figure 5: Simultaneous reduction of the 4/rev hub shears and moment, comparison of ACF and conventional IBC, at μ=0.30 and for ω_{T_1}=3.50

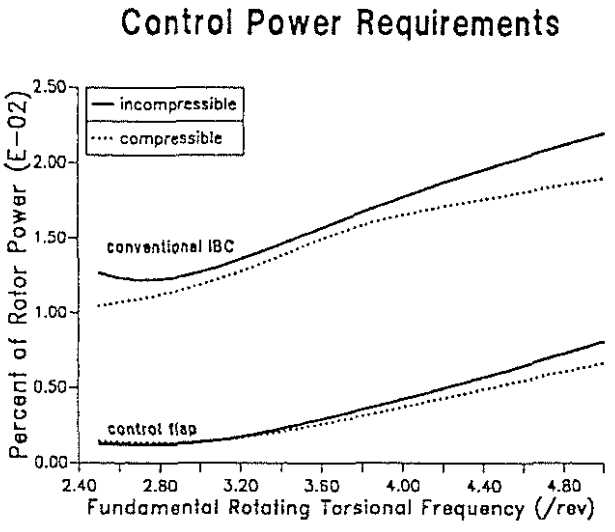

Figure 6: Comparison of power requirements for vibration reduction using actively controlled trailing edge flap and conventional IBC, including effect of compressibility, at μ=0.30

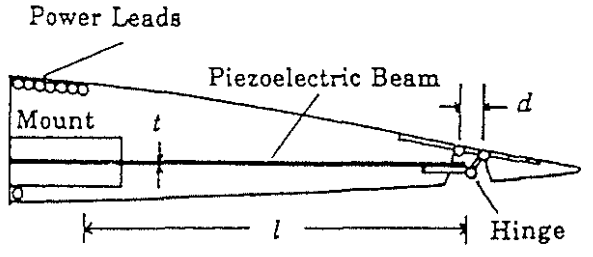

Figure 7: Schematic description of a piezo-bimorph actuated trailing edge flap [48]

Figure 8: Schematic configuration of bimorph and flap geometry, L=length of bimorph bender beam, d=flap lever arm length [20]

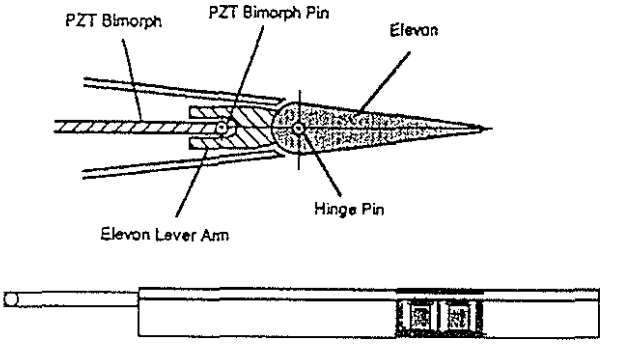

Figure 9: Airfoil cross section with PZT bimorph bender beam and elevon lever mechanism (top); blade planform showing fiberglass spar, active elevon section and PZT actuator layout (bottom) from [20]

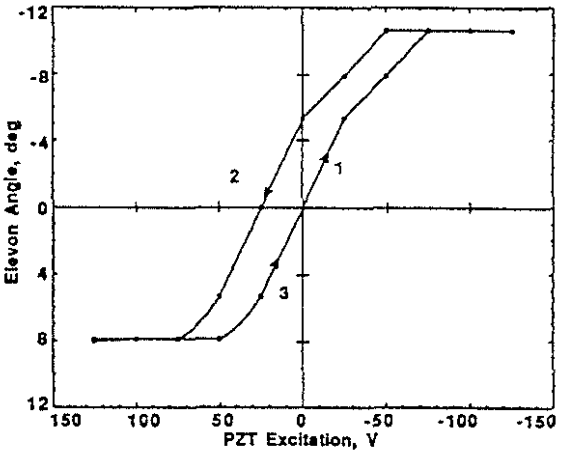

Figure 10: Nonlinear hysteresis characteristics of actuator-flap deflection for blade 1 [20]

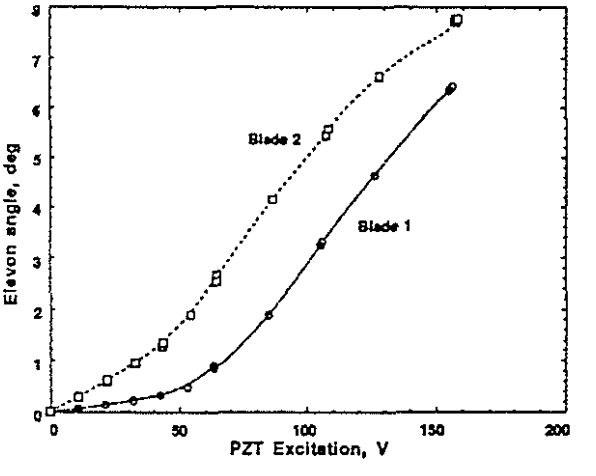

Figure 11: Flap deflection amplitude versus PZT excitation voltage, 760 RPM, 5 Hz, θ_0=3.5 deg. [20]

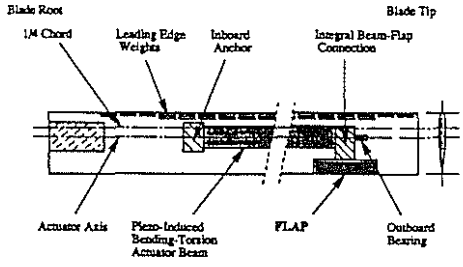

Figure 12: Schematic concept for blade with flap actuated by piezo-induced bending torsion actuator beam [4]

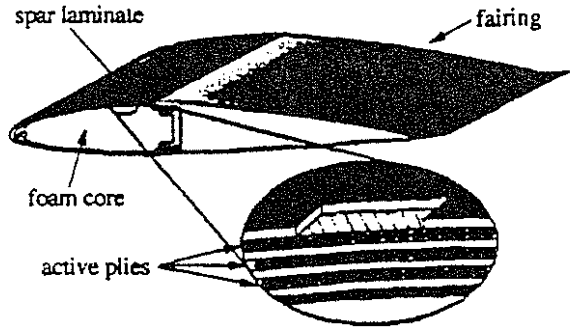

Figure 13: Schematic representation of integrally actuated active twist blade [43]

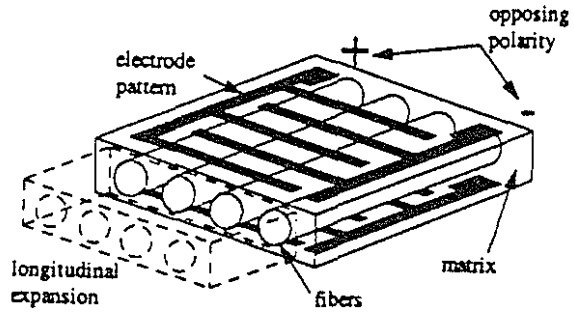

Figure 14: Active fiber composite geometry with interdigitated electrode pattern [43]

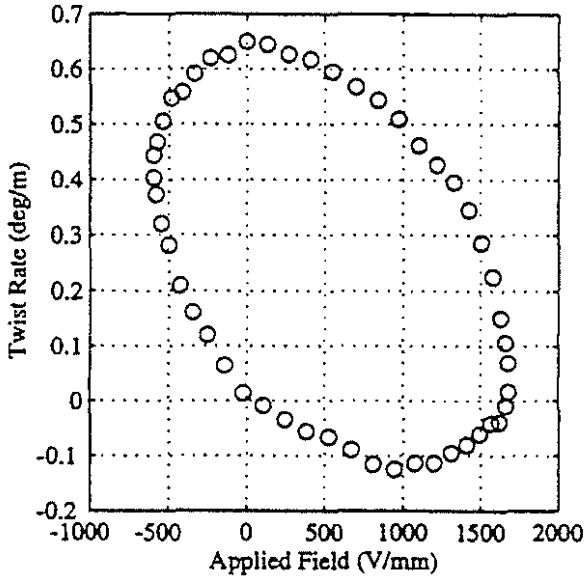

Figure 15: Hysteresis loop for twist rate as a function of applied elastic electric field at 20 Hz [43]